Indian Journal of Chemistry
Vol. 64, November 2025, pp. 1097-1111
DOI: 10.56042/ijc.v64i11.24230

# Synthesis, spectroscopical studies, DFT, ADME, molecular docking analysis, antimalarial, antimicrobial activities of some *E*-imines and XRD structure of (*E*)-*N*-(2-bromobenzylidene)-2-(trifluoromethyl)benzenamine

P Gayathri[†a], Koteswara Rao Anam[a,b], J Divya[a,c], S Balasundari[a], P Sudha[a], P Mayavel[a,d], I Muthuvel[a,e], V Usha[f], V Sathiyendiran[g], B Krishnakumar[†h,i,j], K Ranganathan[k], N Dinesh Kumar[a,l], S Rajasri[m] & G Thirunarayanan*[a]

[a] Department of Chemistry, Annamalai University, Annamalinagar 608 002, India

[b] Department of Chemistry, Acharya Nagarjuna University, Nagarjuna Nagar 522 510, Andra Pradesh, India

[c] Department of Chemistry, Indra Ganesan College of Engineering, Manikandam, Tiruchirappalli 620 012, India

[d] Department of Chemistry, Government Arts College, Ariyalur 621 713, India

[e] Department of Chemistry, M. R. Government Arts College, Mannargudi 614001, India

[f] Department of Chemistry, University College of Engineering Panruti, Panruti 607 106, India

[g] Department of Chemistry, Sourashtra College, Madurai 625 004, India

[h] Saveetha School of Engineering, Saveetha Institute of Medical and Technical Sciences (SIMATS), Chennai 602 105, India

[i] Department of Civil Engineering, Yeungnam University, Gyeongsan, 38541, Republic of Korea

[j] Centre for Research Impact and Outcome, Chitkara University Institute of Engineering and Technology, Chitkara University, Rajpura 140 401, Punjab, India

[k] Department of Chemistry, P. T. Lee Chengalvaraya Naickar College of Engineering and Technology, Kanchipuram 631 502, India

[l] Department of Chemistry, Nanomaterials Laboratory, Kalasalingam Academy of Research and Education, Krishnankoil 626 126, India

[m] Department of Chemistry, Raak College of Engineering and Technology, G. N. Palayam, Villiyanur, Puducherry 605 110, India

E-mail: drgtnarayanan@gmail.com, thirunarayanan.g.10313@annamalaiuniversity.ac.in

*Received 26 September 2025; accepted (revised) 4 November 2025*

Two series of aryl *E*-amines have been synthesised through fly-ash:$Bi_2O_3$-$SO_4^{2-}$ catalyzed aryl amine-aldehyde condensation under ultrasound-promoted, eco-friendly solvent conditions. The reaction affords the target compounds with an excellent yield 80%. The synthesized imines have been thoroughly characterized using elemental (micro) analysis, analytical techniques, and various spectroscopic methods. The molecular structure of *N*-(2-bromobenzylidene)-2-(trifluoromethyl)benzenamine has been unambiguously confirmed through single-crystal X-ray diffraction spectrum. Density Functional Theory (DFT) computations have been utilized to explore the optimized geometries, molecular electrostatic potential maps, and frontier molecular orbitals (FMOs) of the compounds. Mulliken charge distribution analysis has also been conducted to gain insight into the electronic characteristics of the imines. Additionally, ADME predictions provide an initial evaluation of their pharmacokinetic and pharmacodynamic profiles. Molecular docking studies have been conducted to investigate protein-ligand interactions, revealing potential binding affinities within a target protein. The antimicrobial efficacy of the synthesized imines has been further assessed through the Bauer-Kirby disk diffusion approach against a panel of bacterial and fungal strains. *In vitro* studies have been conducted to evaluate the antimalarial potency of these imines against *P. falciparum* Thai strain using a protein-targeted microbial assay system.

**Keywords**: Fly-ash:$Bi_2O_3$-$SO_4^{2-}$, Ultrasonication, *E*-imines, XRD, DFT, ADME, Bio-potencies

The creation of carbon–nitrogen double bonds is essential in organic synthesis and is commonly achieved through the reaction of aldehydes with amines under acidic conditions, leading to the formation of imines, also known as Schiff bases[1]. These Schiff bases-alternatively referred to as imines or azomethines are typically synthesized *via* a straightforward condensation reaction between primary amines and carbonyl containing compounds. Moreover, several studies have demonstrated that naturally occurring molecules bearing azomethine functionalities exhibit significant pharmacological potential[2]. Characteristic functional group (–N=CH–) of Schiff bases have garnered considerable interest due to their extensive biological properties. They are counted among the most widely utilized classes of organic compounds, displaying

† These authors contributed equally to this work.

diverse bioactivities such as antibacterial[3], antifungal[4], antiviral[5], anticancer[6], antioxidant[7], anti-inflammatory[8], anti-tubercular[9], antimycobacterial[10], anticonvulsant[11], antiproliferative[12], anti-HIV[13], hypolipidemic and antihypertensive[5], analgesic[6], cytotoxic[14], lipoxygenase-inhibiting[15], herbicidal[16], insecticidal[17], and antimalarial[18] effects. Conventionally, imines are formed through the reaction between aldehydes or ketones and amines, typically in the presence of an acid catalyst. Alternatively, imines can also be generated *via* the oxidative self-condensation of amines[19]. In traditional synthetic methodologies, the condensation of aldehydes and amines to form imines typically involves the use of unstable aldehydes, amines, dehydrating agents, and Lewis's acid and base catalysts[20], $P_2O_5.SiO_2$ (Ref. 21), Zinc ferrites[22], $ZnFe_2O_4$ (Ref. 23), $FeCl_3$-bentonite[24], $ZnCl_2$ (Ref. 25). Spectroscopic analyses provide valuable insights into the equilibrium states and structural configurations (such as *E*/*Z* isomerism) of organic molecules[26]. Imines and their derivatives serve as important intermediates in organic synthesis, particularly in the construction of heterocycles and non-natural β-amino acids[27]. It is well established that ultrasonic irradiation significantly enhances the rate of various organic transformations. Mayavel *et al*.[28] reported spectral investigations of certain (*E*)-*N*-(4-nitrobenzylidene)-1-benzylpiperidine-4-amines, while Suresh *et al*. synthesized a range of aryl imines under solvent-free conditions and examined the influence of substituted benzylidene-4-methoxyaniline through spectroscopic studies[29]. Moreover, molecular docking analysis offers critical information regarding the binding affinity, free energy changes, and stability of ligand–receptor complexes. Currently, molecular docking techniques are extensively used to predict the potential binding interactions and affinities within ligand–receptor complexes. In this study, *in silico* molecular docking was conducted using various docking tools, including AutoDock software, to determine the most effective method for interaction with the selected target proteins. This research deals with the preparation, structural analysis, and anticancer evaluation of the compounds, along with preliminary results from docking and virtual screening studies[19]. The synthesized molecules in the present study were thoroughly characterized through spectroscopic methods such as IR, NMR, and single-crystal X-ray diffraction, as well as density functional theory (DFT) in B3LYP method 6-311G (d,p) as basic set calculations. Recently, Dinesh Kumar *et al*., investigated the greener synthesis, spectroscopic study, XRD, molecular docking, ADME and *in silico* activities of some *E*-imines[30,31]. Based on the above rationale, authors taken effort to synthesis some *E*-imines and studied the spectroscopical, XRD, computational and *in silico* activities.

## Results and Discussion

### Chemistry of *E*-imines

In this study, the *E*-imines were synthesised by fly-ash:$Bi_2O_3$-$SO_4^{2-}$ catalyst assisted aryl amine–aldehydes condensation under ultrasound-promoted, eco-friendly solvent conditions. This condensation gave more than 95% yields. The electro donating substituents gave more yields than electro-withdrawing substituents. This reaction followed the well-known acidic catalysed mechanism. First step is the protonation aldehydic carbonyl oxygen and the carbonyl carbon gets positive charge. Secondly, this carbon was attached by the nucleophile amine to the positive charged carbonyl carbon of aldehyde and the nitrogen atom gests positive charge. The third step is the removal of proton from the positive nitrogen atom and the nitrogen was neutralized. The fourth one is the removal of water afforded the *E*-imines. These mechanistic steps are illustrated in Scheme 1.

In this reaction the effect of solvent on the yield was studied using acetonitrile, ethanol, methanol, dioxane, dichloromethane and tetrahydrofuran. Among these solvents, ethanol medium gave more yield and THF medium gave lower yields. The effect of solvents on the yields are illustrated in Table 1.

### Single-crystal structure description of (*E*)-N-(2-bromobenzlidene)-2-(trifluoromethyl) Compound 13

Single-crystal X-ray diffraction analysis confirmed that compound **13** crystallizes in a monoclinic crystal system with a $P1_{21/1c}$ space group. The unit cell parameters are a = 10.004(12) Å, b = 7.913(10) Å, c = 16.739(2) Å, with α = β = γ = 90°. The unit cell comprises eight molecules, and the compound adopts an *E*-configuration. Detailed crystallographic measured values and optimization criteria are presented in Table 2. The ORTEP diagram and the DFT-geometry-molecular structure, including atom numbering, are shown in Fig. 1. The crystal packing arrangement derived from experimental data is illustrated in Fig. 2. The theoretical structure optimization was conducted using the B3LYP functional with the 6-311G(d,p) basis set, providing structured bond lengths and bond angles. These theoretical values were relative to the respective experimental values obtained from X-ray analysis, and

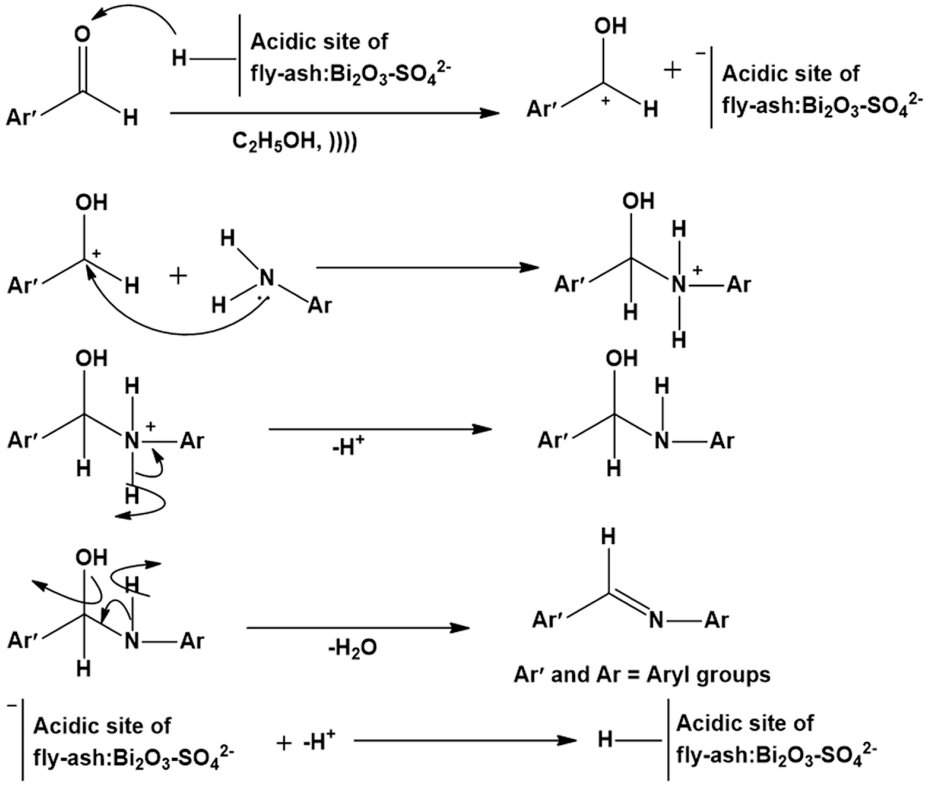


Scheme 1 — The proposed mechanistic route for the synthesised *E*-imine

Table 1 — The influence of solvent on *E*-imines yield (%)

| Solvent→ Entry↓ | ACN | EtOH | MeOH | DO | DCM | THF |
|---|---|---|---|---|---|---|
| **1** | 85 | 96 | 94 | 76 | 72 | 68 |
| **2** | 77 | 89 | 88 | 72 | 68 | 59 |
| **3** | 79 | 81 | 79 | 73 | 59 | 54 |
| **4** | 85 | 99 | 95 | 84 | 63 | 53 |
| **5** | 84 | 99 | 94 | 83 | 68 | 55 |
| **6** | 85 | 99 | 95 | 81 | 69 | 56 |
| **7** | 86 | 92 | 89 | 81 | 70 | 58 |
| **8** | 86 | 99 | 91 | 81 | 69 | 60 |
| **9** | 87 | 99 | 92 | 82 | 68 | 63 |
| **10** | 85 | 99 | 93 | 80 | 70 | 69 |
| **11** | 86 | 99 | 89 | 80 | 70 | 65 |
| **12** | 84 | 90 | 87 | 83 | 69 | 66 |
| **13** | 85 | 96 | 92 | 81 | 69 | 66 |
| **14** | 83 | 88 | 85 | 79 | 71 | 69 |
| **15** | 87 | 93 | 89 | 81 | 72 | 70 |
| **16** | 86 | 93 | 90 | 81 | 73 | 69 |

the results are compiled in Table 3 (See supplementary material for full details).

## DFT analysis of Schiff bases

### Computational optimization of Schiff bases

The structured geometry of the substance was calibrated using the B3LYP method/6-311G basic set, level of theory, converging to a stable minimum energy geometry as confirmed by frequency calculations showing no imaginary frequencies.

### Molecular ESP evaluation of Schiff bases

The molecular electrostatic potential (MEP) functions as a vital descriptor for identifying regions susceptible to electrophilic and nucleophilic

interactions, along with predicting potential hydrogen bonding interactions. The MEP surface also correlates well with key molecular properties such as dipole moment, electronegativity, and chemical reactivity. The MEP distribution of the target compound, as depicted in Fig. 3 was computed using the B3LYP/6-311G(d,p) level of theory. Areas displaying significant positive potential are shown in blue, indicating the most probable nucleophilic attack sites. In contrast, regions with strong negative potential are highlighted in red, representing favourable sites for electrophilic interactions. The MEP surface colour coding is interpreted as follows: red denotes regions of high electron density (partial negative charge), blue signifies electron-deficient zones (partial positive charge), light blue indicates mildly electron-deficient areas, yellow represents slightly electron-rich regions, and green corresponds to areas of neutral electrostatic potential. These colours reflect varying MEP intensities in the order: blue < green < yellow < orange < red. In the MEP profile, blue areas suggest sites of strong electrophilic attraction, while red areas indicate strong repulsion or nucleophilic preference (See supplementary material for MEP diagram of all compounds). Notably, the red zone surrounding the azomethine nitrogen atom (N1) and the yellow region near the bromine atom suggest favourable sites for electrophilic interactions.

Table 2 — Crystal structure and refinement information for Schiff base **13**

| | |
|---|---|
| Empirical formula | $C_{14}H_9BrF_3N$ |
| Formula weight | 328.13 g/mol |
| Temperature | 300(2) K |
| Wavelength | 0.71073 Å |
| Crystal system | Monoclinic |
| Space group | $P1_{21/1c}$ |
| Unit cell dimensions | a=10.0047(12)(2)Å / α=90˚<br>b=7.9137(10)Å/ β=102.161(13)˚<br>c=10.739(2) Å/ $_{\gamma}$=90˚ |
| Volume | 1295.6(3) $Å^3$ |
| Z | 4 |
| Density (calculated) | 1.682 $g/cm^3$ |
| Absorption coefficient | 3.193 $mm^{-1}$ |
| F(000) | 648 |
| Crystal size | 0.145×0.241×0.242 $mm^3$ |
| Theta range for data collection | 2.08 to 28.30° |
| Index ranges | -13<=h<=12, -10<=k<=10, -21<=l<=22 |
| Reflections collected | 29619 |
| Independent reflections | 3208 [R(int.) = 0.0588] |
| Coverage of independent reflections | 99.5% |
| Absorption correction | Multi-scan |
| Refinement method | Full-matrix least-squares on $F^2$ |
| Data / restraints / parameters | 3208 / 0 / 172 |
| Goodness-of-fit on $F^2$ | 1.028 |
| Final R indices [I>2sigma(I)] | R1 = 0.0488, wR2 = 0.1094 |
| R indices (all data) | R1 = 0.0959, wR2 = 0.1285 |
| Largest diff. peak and hole | 0.817 and -0. 764 e.$Å^{-3}$ |
| CCDC Number | 2403616 |

## Frontier molecular orbital analysis of Schiff bases

The Highest Occupied Molecular Orbital (HOMO) and the Lowest Unoccupied Molecular Orbital (LUMO), collectively termed the frontier molecular orbitals (FMOs), are key descriptors in quantum chemical studies. HOMO corresponds to the highest energy orbital containing electrons, revealing that the

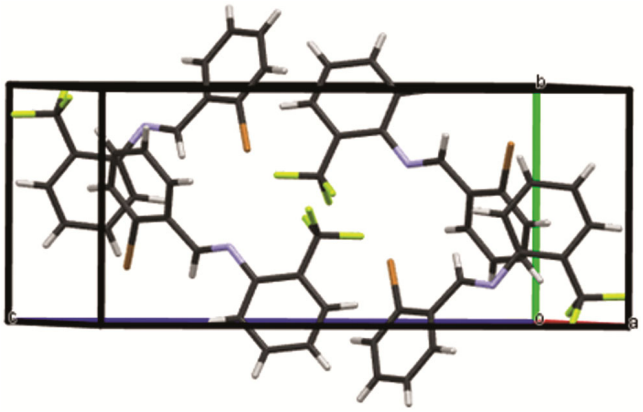


Fig. 2 — Packing diagram of Schiff base 1

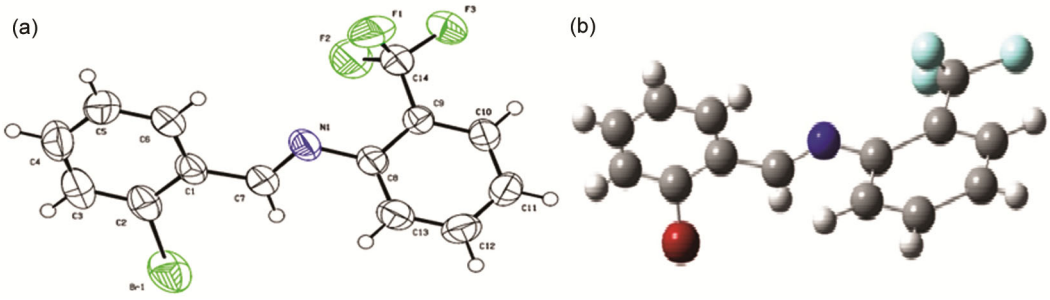


Fig. 1 — The ORTEP (a) and optimized molecular (b) structure of Schiff base 13

Table 3 — Experimental and theoretical bond length and bond angle (°) of compound **13a**

| Bond lengths [Å] | | | | | |
|---|---|---|---|---|---|
| Atom | Bond lengths [Å] | DFT | Atom | Bond lengths [Å] | DFT |
| Br(1)-C(2) | 1.896(4) | 1.345 | C(5)-C(6) | 1.372 | 1.331 |
| F(2)-C(14) | 1.326(4) | 1.905 | C(8)-C(13) | 1.385 | 1.211 |
| N(1)-C(7) | 1.260(4) | 1.312 | C(9)-C(10) | 1.381 | 1.363 |
| F(1)-C(14) | 1.328(4) | 1.186 | C(10)-C(11) | 1.372 | 1.213 |
| F(3)-C(14) | 1.340(4) | 0.943 | C(11)-C(12) | 1.370 | 1.945 |
| N(1)-C(8) | 1.414(4) | 1.378 | C(12)-C(13) | 1.376 | 1.365 |
| C(1)-C(6) | 1.390(5) | 1.002 | C(1)-C(2) | 1.397 | 1.296°° |
| C(1)-C(7) | 1.465(4) | 1.482 | C(2)-C(3) | 1.378 | 1.315 |
| C(3)-C(4) | 1.363(6) | 0.974 | C(8)-(C9) | 1.400 | 1.974 |
| C(4)-C(5) | 1.383(7) | 1.233 | C(9)-C(14) | 1.486 | 1.322 |
| Bond angles [°] | | | | | |
| Atom | XRD | DFT | Atom | XRD | DFT |
| C7-N1-C8 | 118.0(3) | 137.24 | F1-C14-C9 | 112.8(3) | 105.98 |
| C6-C1-C7 | 120.3(3) | 118.28 | C6-C1-C2 | 117.3(3) | 103.36 |
| C3-C2-C1 | 120.9(4) | 136.33 | C2-C1-C7 | 122.4(3) | 138.33 |
| C1-C2-Br1 | 121.1(3) | 112.61 | C3-C2-Br1 | 118.0(3) | 111.04 |
| C3-C4-C5 | 120.2(4) | 108.94 | C4-C3-C2 | 120.3(4) | 116.84 |
| C5-C6-C1 | 121.7(4) | 119.89 | C6-C5-C4 | 119.5(4) | 134.45 |
| C13-C8-C9 | 118.1(3) | 134.29 | N1-C7-C1 | 122.1(3) | 140.87 |
| C9-C8-N1 | 119.3(3) | 140.49 | C13-C8-N1 | 122.6(3) | 85.18 |
| C10-C9-C14 | 119.8(3) | 82.28 | C10-C9-C8 | 119.9(3) | 156.14 |
| C11-C10-C9 | 120.8(3) | 83.154 | C8-C9-C14 | 120.3(3) | 136.37 |
| C11-C12-C13 | 120.2(3) | 135.68 | C12-C11-C10 | 119.7(3) | 135.68 |
| F2-C14-F1 | 106.0(3) | 100.20 | C12-C13-C8 | 121.2(3) | 83.72 |
| F1-C14-F3 | 106.0(3) | 101.13 | F2-C14-F3 | 105.6(3) | 129.48 |
| F2-C14-C9 | 113.5(3) | 83.025 | F3-C14-C9 | 112.4(3) | 132.39 |
| CCDC Number | | | | 2403616 | |

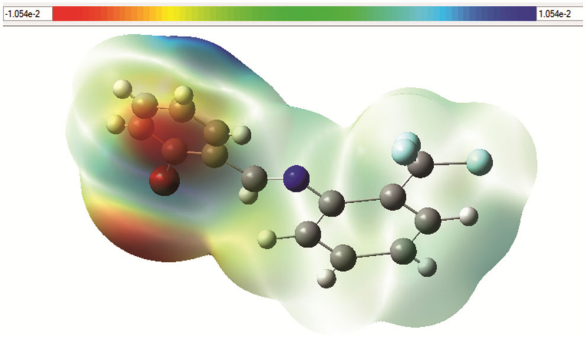


Fig. 3 — The MEP diagram of compound **13**

molecule's electron-donating ability, while LUMO signifies the lowest energy orbital with vacant positions, signifying the potential to accept electrons. Fig. 4 illustrates the computed HOMO and LUMO energy levels using the B3LYP method with the 6-311G(d,p) basis set (See supplementary material HOMO and LUMO energy levels of all compounds). The calculated energy gap between HOMO and LUMO is 1.45 eV, suggesting strong inhibitory potential. Additional global reactivity descriptors are summarized in Table 4.

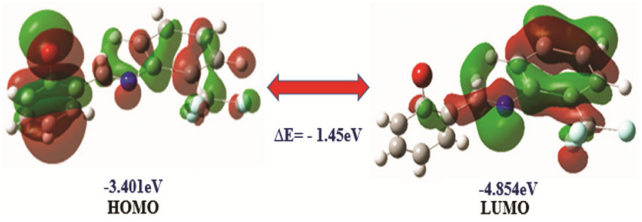


Fig. 4 — HOMO-LUMO energy level of compound **13**

## Mulliken charge analysis of Schiff bases

Mulliken population analysis is one of the most widely used methods for evaluating atomic charges within a molecular framework. This approach estimates the partial charge on each atom and demonstrates how charge distribution whether positive or negative can influence bond lengths across the molecular structure. A review of the literature underscores the crucial role of accurate atomic charge calculations in improving the reliability of quantum mechanical studies of molecular systems. The distribution of Mulliken atomic charges for compound 13 is illustrated graphically in Fig. 5 with the corresponding values presented in Table 5

Table 4 — The HOMO and LUMO of the Schiff bases

| Entry | HOMO | LUMO | Energy Gap (Δ)(eV) | Chemical potential (μ) | Electro-negativity (χ) | Hardness (η) | Softness (S) | Elecro-philicity (ω) |
|---|---|---|---|---|---|---|---|---|
| 1 | –6.068 | –2.367 | 3.684 | 4.228 | –4.228 | 1.842 | 0.271 | 4.853 |
| 2 | –5.714 | –2.966 | 2.761 | 4.350 | –4.350 | 1.381 | 0.362 | 6.850 |
| 3 | –5.741 | –2.775 | 2.960 | 4.277 | –4.277 | 1.480 | 0.338 | 6.180 |
| 4 | –6.149 | –2.394 | 3.774 | 4.287 | –4.287 | 1.887 | 0.265 | 4.870 |
| 5 | –6.503 | –2.612 | 3.894 | 4.581 | –4.581 | 1.947 | 0.257 | 5.389 |
| 6 | –6.286 | –3.102 | 3.194 | 4.705 | –4.705 | 1.597 | 0.313 | 1.597 |
| 7 | –4.789 | –2.095 | 2.694 | 3.450 | –3.450 | 1.347 | 0.371 | 4.419 |
| 8 | –6.394 | –2.585 | 3.809 | 4.498 | –4.498 | 1.905 | 0.263 | 5.311 |
| 9 | –6.340 | –1.823 | 4.517 | 4.103 | –4.103 | 2.258 | 0.221 | 3.728 |
| 10 | –6.231 | –1.714 | 4.520 | 3.985 | –3.985 | 2.260 | 0.221 | 3.513 |
| 11 | –6.095 | –2.258 | 3.817 | 4.189 | –4.189 | 1.908 | 0.261 | 4.597 |
| 12 | –6.449 | –2.014 | 4.449 | 4.241 | –4.449 | 2.224 | 0.225 | 4.042 |
| 13 | –4.843 | –3.401 | 1.453 | –4.128 | –4.128 | 0.727 | 0.688 | 11.726 |
| 14 | –7.047 | –4.925 | 2.122 | 5.986 | –5.986 | 1.061 | –0.261 | 16.884 |
| 15 | –7.292 | –4.626 | 2.667 | 5.959 | –5.959 | 1.333 | –0.261 | 13.317 |
| 16 | –5.905 | –1.932 | 0.145 | 3.924 | –3.924 | 1.984 | 0.252 | 3.881 |

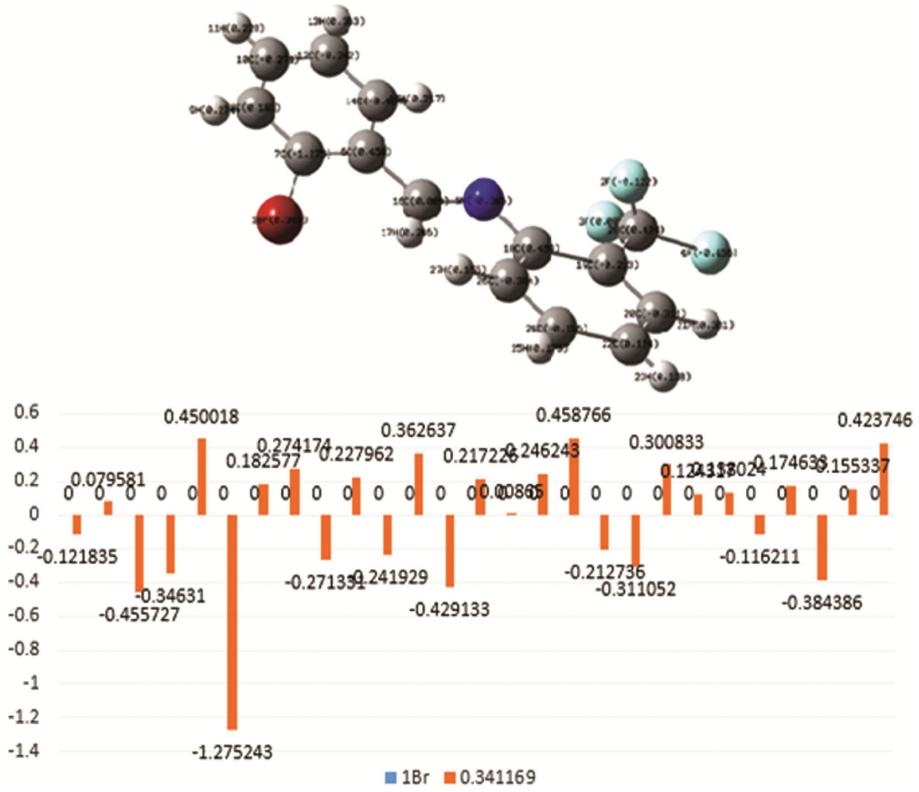


Fig. 5 — The Mulliken charge and the atoms of *E*-imine **13**

(See supplementary material for Mulliken charges of all compounds). According to this table, atoms $F_2$, $F_4$, and $N_5$, along with carbon atoms $C_7$, $C_{10}$, $C_{12}$, $C_{19}$, $C_{20}$, and $C_{24}$, carry negative charges and therefore act as donor atoms particularly the highly electronegative fluorine atom $F_4$ (–0.455). In contrast, carbon atoms $C_6$, $C_8$, $C_{16}$, $C_{22}$, and $C_{28}$ have positive charges and function as acceptor atoms, especially the highly electronegative carbon atom $C_{18}$, which bears a positive charge of 0.458e.

Table 5 — Calculated Mullikan atomic charge of Schiff bases compound **13**

| Atom | Charge |
|---|---|
| Br1 | 0.344 |
| F2 | –0.121 |
| F3 | 0.079 |
| F4 | –0.455 |
| N5 | –0.346 |
| C6 | 0.450 |
| C7 | –1.275 |
| C8 | 0.182 |
| H9 | 0.274 |
| C10 | –0.271 |
| H11 | 0.227 |
| C12 | –0.241 |
| H13 | 0.362 |
| C14 | –0.429 |
| H15 | 0.217 |
| C16 | 0.008 |
| H17 | 0.246 |
| C18 | 0.458 |
| C19 | –0.212 |
| C20 | –0.311 |
| H21 | 0.300 |
| C22 | 0.124 |
| H23 | 0.138 |
| C24 | –0.116 |
| H25 | 0.174 |
| C26 | –0.384 |
| H27 | 0.155 |
| C28 | 0.423 |

## Molecular docking result

To evaluate the molecular interactions and binding affinities among the synthesized compounds and the bacterial protein target in three-dimensional space, molecular docking was performed by positioning the ligands within the active site of the receptor. AutoDock Vina, following our previously established protocol, was employed for docking studies using the crystal structure of the human estrogen receptor (PDB ID: 3ERT). The docking analysis of imine derivatives (compounds 1–14) demonstrated their ability to interact with the 3ERT receptor, yielding binding energy values region from **–7.89 to –5.22** kcal/mol. Notably, compounds **1, 3, 6** and **16** exhibited the most favourable binding energies, with values of **–7.89** and for compounds **1,** respectively. Compound engaged in electrostatic interactions with GLU B:523 (glutamic acid) and formed hydrophobic interactions with LEU B:525, MET B:522, and LEU B:536. Similarly, compound **3** binding energy value **–8.41** kcal/mol and interacted *via* electrostatic and hydrophobic forces with key amino acid residues including TRP B:383, LEU B:536, MET B:522, LEU B:525, PRO B:535, and VAL B:533. Compound **6** binding energy value **–7.54** kcal/mol and demonstrated interactions with amino acid residues LEU B:391, ARG B:394, TRP B:393, GLY B:390, PRO B:324, and LEU B:328, involving both electrostatic and hydrophobic bonding. Similarly, compound **16** binding energy value **–7.67** kcal/mol and formed interactions with LEU B:539, VAL B:533, LEU B:529, LYS B:529, LEU B:525, and MET B:522, also exhibiting a combination of electrostatic and hydrophobic interactions. These docking outcomes are likely influenced by the presence of halogen substituents within the molecular framework. The corresponding 2D and 3D visualizations of the top-binding compounds **(1, 3, 6,** and **16)** are presented in Table 6 (See supplementary material for 2D and 3D geometries of all compounds).

## Drug-like characteristics and ADME analysis

The safety and efficacy of lead compounds are primarily determined through comprehensive pharmacological evaluations. *In silico* tools, such as the SwissADME web server, offer early predictions of critical physicochemical properties, ADME parameters, and drug-likeness, which are vital components of the drug discovery pipeline. These parameters play a crucial role in screening potential drug candidates, with particular emphasis on compliance with Lipinski's Rule of Five. The complete ADME profile of *E*-imines were presented in Table 7. Compounds that do not meet these criteria are typically considered to lack drug-like characteristics. In the present analysis, the compounds exhibited log P values ranging from 2.93 to 6.14 (ideally <5), molecular weights between 190 and 362 g/mol (≤500 g/mol), hydrogen bond donors ranging from 0 to 3 (≤5), and hydrogen bond acceptors from 2 to 6 (≤10), indicating favourable drug-like profiles. Lipinski's Rule of Five functions as a fundamental criterion for assessing the drug-likeness of compounds, especially in predicting their potential for oral bioavailability in humans based on key physicochemical properties. The biological activity of the synthesized compounds was assessed using Molinspiration Cheminformatics, which classifies compounds as inactive if their activity scores fall below –0.5. All synthesized derivatives demonstrated a bioavailability score of 0.55, indicating moderate biological activity. Notably, compounds 10 and 12 exhibited favourable bioavailability profiles. The bioavailability radar structure was employed to provide a preliminary

Table 6 — The 2D and 3D docking poses with binding energies of *E*-imines

| Compd | 3D docking pose | 2D docking pose | Binding Energy ΔG (Kcal /mol) |
|---|---|---|---|
| **1** | 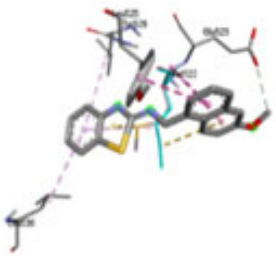 | 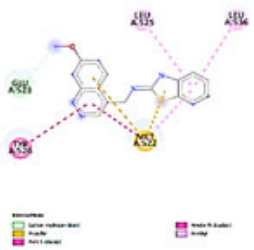 | –7.89 |
| **3** | 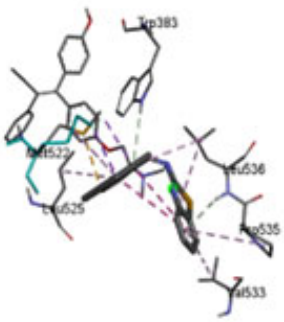 |  | –8.41 |
| **6** | 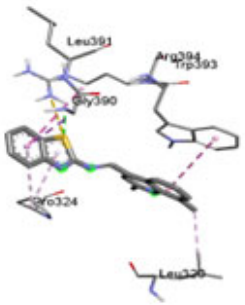 | 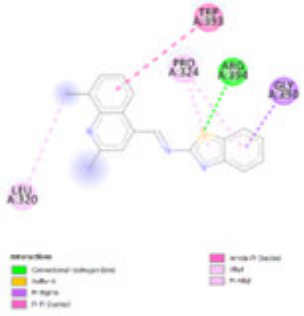 | –7.54 |
| **16** | 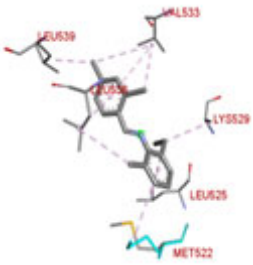 | 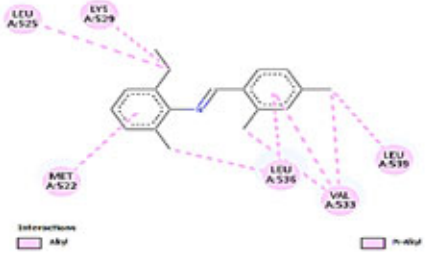 | –7.67 |

visualization of drug-likeness, where the shaded pink region denotes the optimal physicochemical space and are illustrated in Fig. 6 (See supplementary material for ADME Radar pictures of all compounds).

## Antimalarial activities

Measured antimalarial potencies of *E*-imines are presented in Table 8. *E*-imines **6** and **16** shows more antimalarial activity. Compounds **1, 2, 5, 8** and **13** shows moderate antimalarial activity. Remaining compounds shows least antimalarial activities. Here the +I effect of bromine, chlorine, mesomeric effect of methyl, -I effect of methoxy, anthracene and 2-thienyl groups enhances the antimalarial activity.

## Antimicrobial potencies

Assessed antibacterial potencies by the measurement of mm of zone of inhibition was tabulated in Table 9. The MIC values of each compound was given in parentheses. The statistical

Table 7 — Complete ADME profile of *E*-imines

| Compd | Mol. Wt. | Mol. Wt. | Number of H-acceptor | Number of H-donor | TPSA (Å) | Consensus Log $P_o/w$ | Bioavailability Score | Lipinski Criteria |
|---|---|---|---|---|---|---|---|---|
| **1** | $C_{19}H_{14}N_2OS$ | 318 | 3 | 3 | 62.72 | 4.77 | 0.55 | 0 |
| **2** | $C_{22}H_{14}N_2S$ | 338 | 2 | 2 | 53.49 | 5.61 | 0.55 | 1 |
| **3** | $C_{24}H_{14}N_2S$ | 362 | 2 | 0 | 53.49 | 6.14 | 0.55 | 1 |
| **4** | $C_{12}H_8N_2OS$ | 228 | 3 | 0 | 66.63 | 3.20 | 0.55 | 0 |
| **5** | $C_{12}H_8N_2S_2$ | 244 | 2 | 0 | 81.73 | 3.91 | 0.55 | 0 |
| **6** | $C_{18}H_{12}ClN_3S$ | 338 | 3 | 0 | 66.38 | 5.06 | 0.55 | 0 |
| **7** | $C_{17}H_{13}N_3OS$ | 307 | 3 | 1 | 78.51 | 4.11 | 0.55 | 1 |
| **8** | $C_{10}H_{11}ClN_2S$ | 287 | 2 | 0 | 53.49 | 4.53 | 0.55 | 1 |
| **9** | $C_{10}H_{10}N_2S$ | 190 | 2 | 0 | 53.49 | 2.93 | 0.55 | 0 |
| **10** | $C_{13}H_{14}N_2S$ | 230 | 2 | 0 | 53.49 | 3.76 | 0.55 | 1 |
| **11** | $C_{20}H_{14}N_2S$ | 314 | 2 | 0 | 53.49 | 5.04 | 0.55 | 0 |
| **12** | $C_{17}H_{20}N_2S$ | 294 | 2 | 1 | 53.49 | 4.70 | 0.55 | 1 |
| **13** | $C_{14}H_{19}BrF_3N$ | 326 | 4 | 0 | 12.36 | 4.88 | 0.55 | 1 |
| **14** | $C_{14}H_9F_3N_2O_2$ | 294 | 6 | 1 | 62.02 | 2.24 | 0.55 | 0 |
| **15** | $C_{14}H_9F_3N_2O_2$ | 295 | 6 | 1 | 62.02 | 2.70 | 0.55 | 0 |
| **16** | $C_{16}H_{15}Cl_2N$ | 292 | 1 | 0 | 12.36 | 5.23 | 0.55 | 1 |

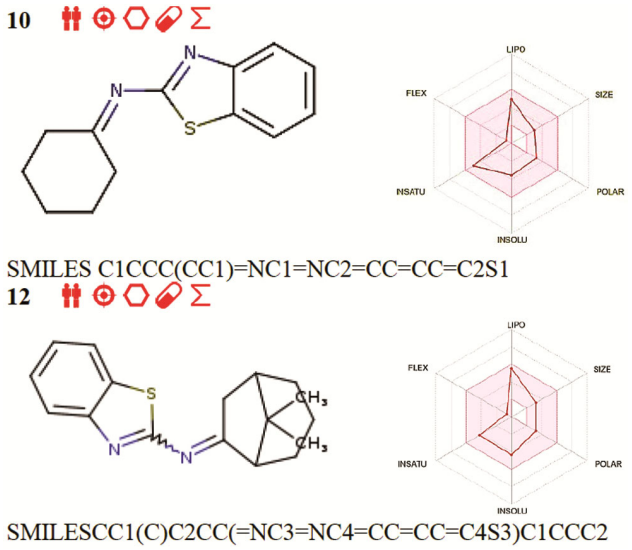


Fig. 6 — The bioavailability radar of the compounds **10** and **12**

column chart representation of antibacterial activities was illustrated in Fig. 7. All *E*-imines exists excellent and good antibacterial potencies against all antimicrobial strains. The -I effect of methoxy and aryl groups, +I effect of bromo-, chloro-, ethyl, mesomeric effect of methyl and positive character of nitro groups are enhancing the antibacterial activities.

### Antifungal potencies

Assessed antifungal potencies by the measurement of mm of zone of inhibition was tabulated in Table 9. The MIC values of each compound was given in parenthesis's statistical column chart was illustrated in Fig. 8. All *E*-imines exists excellent and good antibacterial potencies against *C. albicans* and *P. chrysogenum* antifungal strains. The -I effect of methoxy and aryl groups, +I effect of bromo-, chloro- and positive character of nitro groups are enhancing the antibacterial activities. *E*-imines **1, 2, 8** and **13-16** were shown good anti-fungal activity against *A. niger strain* and *A. fumigatus strains.* Here the -I effect of methoxy, +I effect of bromine, chloride, anthracene ring, electronegative character of fluorine, positive character of nitro group and mesomeric effect of methyl groups enhanced the antifungal activity. The remaining *E*-imines show moderate antifungal activity.

## Experimental Section

### Materials and Methods

All chemicals used in this study was procured from Sigma-Aldrich Chemical Company. Reaction performance was monitored by Thin Layer Chromatography (TLC). The melting points of the synthesized compounds were determined using a Suntex melting point apparatus, and the data's reported are uncorrected. Fourier-transform infrared (FT-IR) analysis of the imines were measured using an Avatar-300 Thermo Nicolet spectrophotometer in the range of 4000–400 $cm^{-1}$, employing potassium bromide (KBr) pellets. The $^1H$ and $^{13}C$ NMR spectra were obtained on a BRUKER AVANCE III 400 MHz

Table 8 — Assessed antimalarial activities of *E*-imines

| Entry | Ar | Ar′ | Antimalarial potency |
|---|---|---|---|
| 1 | 2-Aminobenzo[d]thiazole | 6-Methoxy-1-naphthyl | 35±0.28 |
| 2 | 2-Aminobenzo[d]thiazole | 9-Anthracenyl | 36±0.21 |
| 3 | 2-Aminobenzo[d]thiazole | 1-Pyrenyl | 34±0.66 |
| 4 | 2-Aminobenzo[d]thiazole | 2-Furanyl | 24±0.38 |
| 5 | 2-Aminobenzo[d]thiazole | 2-Thiophenyl | 36±0.21 |
| 6 | 2-Aminobenzo[d]thiazole | 2-Chloro-8-methyl-4-quinolinyl | 40±0.23 |
| 7 | 2-Aminobenzo[d]thiazole | 5-Methoxy-3-indolyl | 33±0.62 |
| 8 | 2-Aminobenzo[d]thiazole | 4-Chlorophenyl | 39±0.36 |
| 9 | 2-Aminobenzo[d]thiazole | Acetone | 30±0.13 |
| 10 | 2-Aminobenzo[d]thiazole | Cyclohexanone | 26±0.22 |
| 11 | 2-Aminobenzo[d]thiazole | Benzophenone | 24±0.33 |
| 12 | 2-Aminobenzo[d]thiazole | Camphor | 20±0.33 |
| 13 | 2-Trifluoromethylaniline | 2–Bromophenyl | 38±0.03 |
| 14 | 2-Trifluoromethylaniline | 3–Nitrophenyl | 29±0.13 |
| 15 | 3-Trifluoromethylaniline | 4–Nitrophenyl | 25±0.09 |
| 16 | 2–Ethyl–6–methylaniline | 2,4–Dichlorophenyl | 42±0.03 |

Table 9 — Antimicrobial activities of *E*-Imines.

| Entry | Zone of inhibition(mm) | | | | | | | | | | | |
|---|---|---|---|---|---|---|---|---|---|---|---|---|
| | Antibacterial activities | | | | | | | | Antifungal activities | | | |
| | Gram positive microbes | | | | | Gram negative microbes | | | Gram positive fungi | | Gram negative fungi | |
| | *B. subtilis* | *E. faecalis* | *S. pneumoniae* | *S. aureus* | *E. coli* | *K, pneumoniae* | *P. mirabilis* | *P. aeruginosa* | *C. albicans* | *P. chrysogenum* | *A. niger* | *A. fumigatus* |
| 1 | 18(20) | 10(25) | 16(30) | 14(25) | 11(25) | 12(20) | 11(20) | 17(25) | 15(30) | 15(30) | 16((25) | 17(20) |
| 2 | 19(25) | 12(30) | 16(25) | 17(20) | 13(25) | 15(25) | 13(20) | 13(25) | 10(30) | 14(20) | 13(25) | 15(20) |
| 3 | 20(30) | 11(25) | 17(25) | 16(20) | 12(20) | 11(30) | 11(20) | 15(20) | 11(20) | 13(20) | 12(25) | 11(25) |
| 4 | 19(25) | 10(25) | 18(20) | 17(25) | 15(20) | 14(30) | 10(30) | 17(20) | 10(20) | 19(25) | 10(20) | 12(25) |
| 5 | 20(20) | 11(25) | 17(20) | 16(25) | 16(20) | 18(30) | 17(30) | 14(20) | 10(20) | 16(30) | 11(20) | 13(25) |
| 6 | 23(20) | 13(20) | 16(25) | 13(25) | 13(30) | 14(25) | 18(30) | 16(30) | 12(25) | 19(30) | 12(25) | 11(30) |
| 7 | 10(20) | 12(20) | 23(30) | 15(30) | 20(30) | 11(25) | 11(25) | 14(30) | 19(25) | 19(25) | 13(30) | 13(30) |
| 8 | 11(25) | 11(30) | 19(20) | 16(30) | 18(30) | 13(25) | 13(25) | 12(25) | 15(30) | 22(25) | 14(30) | 12(25) |
| 9 | 12(20) | 15(30) | 19(25) | 14(30) | 17(25) | 11(20) | 11(25) | 11(30) | 12(30) | 20(30) | 10(30) | 11(20) |
| 10 | 10(30) | 13(30) | 18(25) | 13(20) | 16(25) | 12(20) | 14(25) | 10(20) | 13(20) | 21(30) | 12(20) | 14(20) |
| 11 | 11(25) | 14(25) | 17(25) | 14(20) | 19(25) | 13(20) | 12(20) | 12(20) | 12(25) | 19(20) | 11(20) | 13(25) |
| 12 | 10(20) | 10(25) | 19(20) | 11(20) | 18(20) | 10(25) | 10(20) | 10(25) | 11(30) | 22(20) | 12(25) | 11(30) |
| 13 | 12(30) | 11(20) | 16(30) | 13(20) | 14(25) | 12(25) | 12(20) | 13(30) | 13(30) | 15(20) | 17(20) | 18(20) |
| 14 | 12(25) | 10(20) | 17(30) | 13(25) | 15(309 | 12(30) | 11(30) | 11(30) | 12(20) | 14(25) | 16(20) | 17(30) |
| 15 | 11(30) | 9(25) | 15(25) | 14(30) | 13(20) | 11(30) | 9(20) | 12(25) | 10(25) | 16(25) | 18(20) | 19(25) |
| 16 | 13(30) | 11(30) | 16(20) | 12(30) | 14(25) | 11(25) | 10(25) | 13(20) | 12(30) | 15(25) | 15(20) | 17(30) |
| Std | Ceftazidime | | | | | | | | Clotrimazole | | | |
| | 13 | 11 | 17 | 14 | 15 | 13 | 12 | 14 | 13 | 16 | 18 | 19 |

NMR spectrometer, functioning at 400 MHz for $^{1}H$ and 100 MHz for $^{13}C$, through $CDCl_3$ functioned as the solvent and tetramethylsilane (TMS) as the internal reference. Elemental analysis was carried out in The suitable single crystal (13) was chosen, its lattice constants and diffraction intensities were acquired from BRUCKER AXS single-crystal diffract meter with Mo K αradiation ( λ= 0.71073) at 302(2) K. The structure was solved by the direct method procedure and the non-hydrogen atoms were subjected to anisotropic refinement by full-matrix least-squares on F2 using SHELXL –2016. CNH analyser. The Mass spectra of *E*-imines were measured in Vario mass spectrometer.

## General synthetic methodology for *E*-imines 1–16

An equimolar volume of aryl amines (1 mmol), substituted benzaldehydes (1 mmol) and 0.45g of nano Fly-ash:$Bi_2O_3$-$SO_4^{2-}$ catalyst[32] were subjected to ultrasonic irradiation in 20 mL of ethanol using an ultrasonication bath operating at 40 Hz (Citizen Ultra Sonicator, 40 Hz, 120 Hz, 240 V AC) at ambient temperature for 15–25 minutes (Scheme 2). Thin-layer chromatography (TLC) was employed to observe the reaction progress. After completion, the resulting product were isolated by simple filtration, and the ethanol were evaporated to obtain the crude imine. The substance was recovered by washing with ethyl acetate and recycled in subsequent reactions. The initial

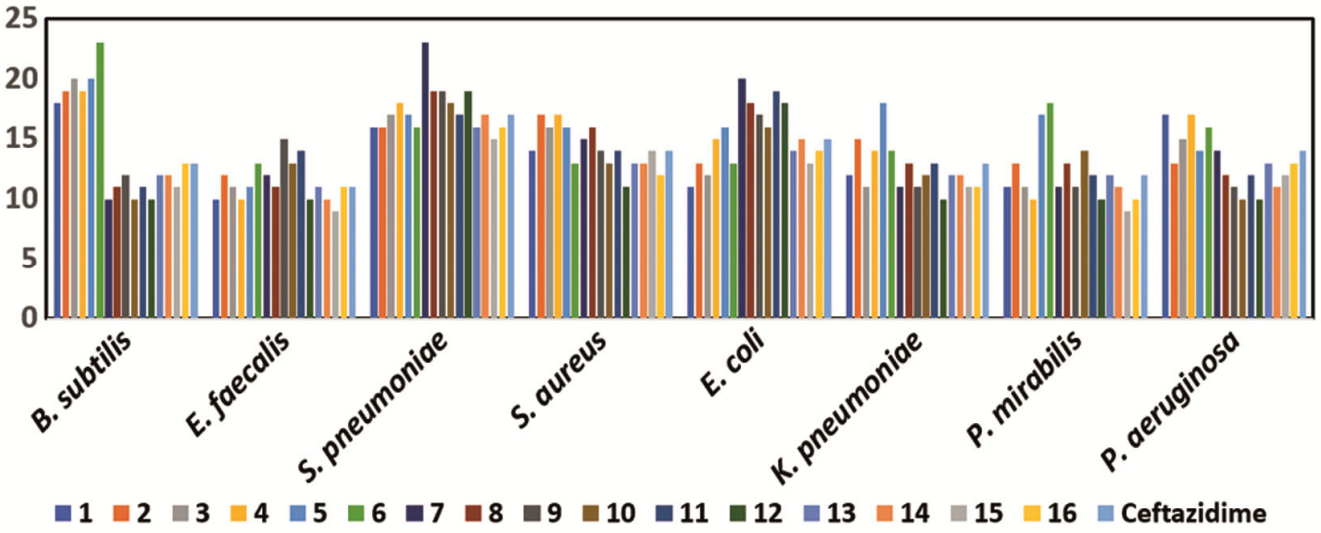


Fig. 7 — Clustered column chart representation of antibacterial activities of *E*-imines

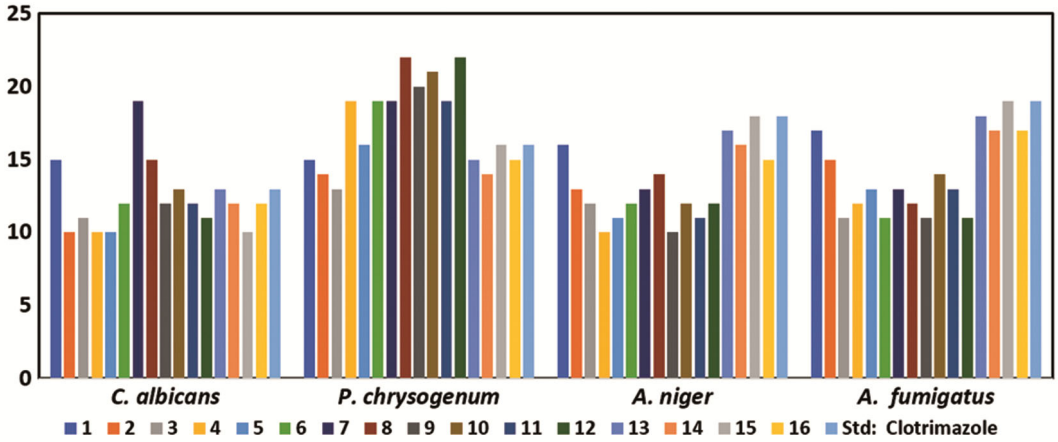


Fig. 8 — Clustered column chart representation of antifungal activities of *E*-imines

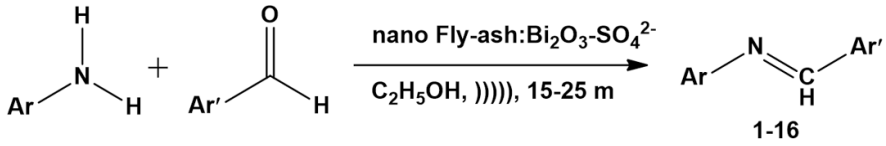


Scheme 2 — Synthesis of *E*-imines by nano Fly-ash:$Bi_2O_3$-$SO_4^{2-}$ catalyst assisted ultrasonicated condensation of aryl amine and aryl carbonyl compounds

product was purified through recrystallization in ethanol, yielding the desired *E*-imines. The compound 13 obtained as a crystal system. The reaction time, yield, and physical properties of the synthesized imines are summarized in Table 10.

The purities of the synthesised *E*-imines (1-12) were analysed with their data reported in literature. These data are fully aggregable. The *E*-imines **(13-16)** were analysed with spectroscopical data are summarised below.

**(*E*)-*N*-(2-Bromobenzylidene)-2-(trifluoromethyl) benzenamine, 13**: IR (KBr): 1580(C = N), 3071 (C-H arom), 1371 $cm^{-1}$ (C-F); $^1$H NMR (400 MHz, $CDCl_3$): δ 8.78(s, 1H), 7.09–7.71(m, 8H, Ar-H); $^{13}$C NMR (100 MHz, $CDCl_3$): δ 160.54, 150.32, 122.56–134.25. Mol. Formula $C_{14}H_9BrF_3N$; MS: *m/z* 326[$M^+$], 328[$M^{2+}$], 330[$M^{4+}$], 257, 248, 181, 172, 154,145, 78, 68, 28, 15. Anal. Calcd: C, 51.53; H, 5.82; N, 4.29. Found: C, 51.56; H, 5.84; N, 4.25%.

Table 10 — The physiochemical constant time and yields of the synthesized imines **1-16**

| Entry | Ar | Ar′ | Mol. Formula | Mol. Wt. | Yield (%) | Time (min) | m.p. (°C) |
|---|---|---|---|---|---|---|---|
| 1 | 2-Aminobenzo[d]thiazole | 6-Methoxy-1-naphthyl | $C_{19}H_{14}N_2OS$ | 318 | 97 | 16 | 208-209(206-209)[33] |
| 2 | 2-Aminobenzo[d]thiazole | 9-Anthracenyl | $C_{22}H_{14}N_2S$ | 338 | 89 | 19 | 216-217(214-216)[33] |
| 3 | 2-Aminobenzo[d]thiazole | 1-Pyrenyl | $C_{24}H_{14}N_2S$ | 362 | 81 | 20 | 223-224(221-223)[33] |
| 4 | 2-Aminobenzo[d]thiazole | 2-Furanyl | $C_{12}H_8N_2OS$ | 228 | 96 | 15 | 164-165(163-165)[33] |
| 5 | 2-Aminobenzo[d]thiazole | 2-Thiophenyl | $C_{12}H_8N_2S_2$ | 244 | 99 | 16 | 173-174(172-173)[33] |
| 6 | 2-Aminobenzo[d]thiazole | 2-Chloro-8-methyl-4-quinolinyl | $C_{18}H_{12}CIN_3S$ | 338 | 99 | 22 | 192-193(190-192)[33] |
| 7 | 2-Aminobenzo[d]thiazole | 5-Methoxy-3-indolyl | $C_{17}H_{13}N_3O$ | 307 | 92 | 19 | 189-190(187-189)[33] |
| 8 | 2-Aminobenzo[d]thiazole | 4-Chlorophenyl | $C_{10}H_{10}N_2S$ | 190 | 99 | 18 | 99-1010(98-99)[33] |
| 9 | 2-Aminobenzo[d]thiazole | Acetone | $C_{13}H_{14}N_2S$ | 230 | 99 | 15 | 113-114(112-113)[33] |
| 10 | 2-Aminobenzo[d]thiazole | Cyclohexanone | $C_{20}H_{14}N_2S$ | 314 | 99 | 23 | 114-115(112-113)[33] |
| 11 | 2-Aminobenzo[d]thiazole | Benzophenone | C20H14 | 314 | 99 | 25 | 120-121(119-120)[33] |
| 12 | 2-Aminobenzo[d]thiazole | Camphor | $C_{17}H_{20}N_2S$ | 284 | 90 | 25 | 222-224(221-223)[33] |
| 13 | 2-Trifluoromethylaniline | 2–Bromophenyl | $C_{14}H_9BrF_3N$ | 326 | 96 | 20 | 176-177 |
| 14 | 2-Trifluoromethylaniline | 3–Nitrophenyl | $C_{14}H_9F_3N_2O_2$ | 294 | 88 | 24 | 132-133 |
| 15 | 3-Trifluoromethylaniline | 4–Nitrophenyl | $C_{14}H_9F_3N_2O_2$ | 294 | 93 | 22 | 163-164 |
| 16 | 2–Ethyl–6–methylaniline | 2,4–Dichlorophenyl | $C_{16}H_{15}Cl_2N$ | 292 | 93 | 24 | 148-150 |

**(*E*)-*N*-(3-Nitrobenzylidene)-2-(trifluoromethyl) benzenamine, 14**: IR (KBr): 1580(C = N), 3078(C-H arom), 1312 $cm^{-1}$ (C-F); $^1H$ NMR (400 MHz, $CDCl_3$): δ 8.69(s, 1H), 7.06–8.46 (m, 8H, Ar-H); $^{13}C$ NMR (100 MHz, $CDCl_3$): δ 158.75, 148.70, 119.30–137.38. Mol. Formula $C_{14}H_9F_3N_2O_2$; MS: *m/z* 294[$M^+$], 296[$M^{2+}$], 298[$M^{4+}$], 248, 179,149, 145, 128, 79, 68, 45, 27, 15. Anal. Calcd: C, 57.14; H, 3.06; N, 9.52. Found: C, 57.18; H, 3.04; N, 9.54%.

**(*E*)-*N*-(4-Nitrobenzylidene)-3-(trifluoromethyl) benzenamine, 15**: IR (KBr): 1693(C = N), 2918(C-H arom), 1345 $cm^{-1}$ (C-F); $^1H$ NMR (400 MHz, $CDCl_3$): δ 8.57(s, 1H), 7.26–8.35 (m, 8H, Ar-H); $^{13}C$ NMR (100 MHz, $CDCl_3$): δ 158.95, 151.32, 117.83–131.89. Mol. Formula $C_{14}H_9F_3N_2O_2$; MS: *m/z* 294[$M^+$], 296[$M^{2+}$], 298[$M^{4+}$], 248, 179,149, 145, 137, 128, 116, 104, 104, 79, 68, 45, 40, 27, 15. Anal. Calcd: C, 57.14; H, 3.06; N, 9.52. Found: C, 57.11; H, 3.08; N, 9.56%.

**(*E*)-*N*-(2,4-Dichlorobenzylidene)-2-(ethyl-6-methyl) benzenamine, 16**: IR (KBr): 1695(C = N), 3088(C-H arom), 1585 $cm^{-1}$ (C-Cl); $^1H$ NMR (400 MHz, $CDCl_3$): δ 1.145(t, 2H), 2.14(s, 3H), 2.51(q, 3H), 8.61(s, 1H), 6.99-8.24 (m, 6H, Ar-H); $^{13}C$ NMR (100 MHz, $CDCl_3$): δ 158.49, 150.40, 124.27–141.13, 24.70, 18.48, 14.70. Mol. Formula $C_{16}H_{15}Cl_2N$; MS: *m/z* 292[$M^+$], 294 [$M^{+2}$], 296[$M^{+4}$]262, 254, 242, 171, 146, 135, 128, 119, 105, 93, 62, 54, 37, 27, 15. Anal. Calcd: C, 65.75; H, 5.13; N, 4.79. Found: C, 65.77; H, 5.09; N, 4.72%.

## Computational studies

Computational studies for compounds 1–16 were performed using GAUSSIAN 09W software, applying Density Functional Theory (DFT) with the B3LYP functional and the 6-311G(d,p) basis set. Molecular structures were rendered using GAUSSVIEW 5.0. Molecular docking simulations were executed with AutoDock 4.0, utilizing various stochastic search techniques; the Lamarckian Genetic Algorithm (LGA) was selected as the optimization protocol. Two-dimensional interaction diagrams were created using the PDBsum web server, while three-dimensional representations were produced with Discovery Studio. Drug-likeness and ADME properties were assessed using the Swiss ADME platform[34].

## Molecular docking analysis

Molecular docking studies of various substituted imine derivatives with the breast cancer target protein were conducted using AutoDock Tools version 1.5.7 (Ref. 35). The crystallographic structure of the human estrogen receptor (PDB ID: 3ERT) was obtained from the Protein Data Bank (PDB) and served as the receptor model in this investigation. The docking protocol was designed to predict the optimal binding conformations of ligand–receptor complexes by minimizing interaction energies, utilizing multiple

Table 11 — Molecular Docking binding energy values of compounds **1–16**

| Entry | Ar | Ar′ | PDB | Binding Energy ΔG(Kcal/mol) |
|---|---|---|---|---|
| 1 | 2-Aminobenzo[d]thiazole | 6-Methoxy-1-naphthyl | 3ERT | –7.89 |
| 2 | 2-Aminobenzo[d]thiazole | 9-Anthracenyl | 3ERT | –6.98 |
| 3 | 2-Aminobenzo[d]thiazole | 1-Pyrenyl | 3ERT | –8.41 |
| 4 | 2-Aminobenzo[d]thiazole | 2-Furanyl | 3ERT | –4.92 |
| 5 | 2-Aminobenzo[d]thiazole | 2-Thiophenyl | 3ERT | –5.91 |
| 6 | 2-Aminobenzo[d]thiazole | 2-Chloro-8-methyl-4-quinolinyl | 3ERT | –7.54 |
| 7 | 2-Aminobenzo[d]thiazole | 5-Methoxy-3-indolyl | 3ERT | –7.15 |
| 8 | 2-Aminobenzo[d]thiazole | 4-Chlorophenyl | 3ERT | –6.95 |
| 9 | 2-Aminobenzo[d]thiazole | Acetone | 3ERT | –5.17 |
| 10 | 2-Aminobenzo[d]thiazole | Cyclohexanone | 3ERT | –5.53 |
| 11 | 2-Aminobenzo[d]thiazole | Benzophenone | 3ERT | –7.21 |
| 12 | 2-Aminobenzo[d]thiazole | Camphor | 3ERT | –6.67 |
| 13 | 2-Trifluoromethylaniline | 2–Bromophenyl | 3ERT | –4.12 |
| 14 | 2-Trifluoromethylaniline | 3–Nitrophenyl | 3ERT | –5.12 |
| 15 | 3-Trifluoromethylaniline | 4–Nitrophenyl | 3ERT | –5.22 |
| 16 | 2–Ethyl–6–methylaniline | 2,4–Dichlorophenyl | 3ERT | –7.67 |

scoring functions. The ligand structures were initially constructed in CDX format through Chem Draw Ultra 12.0. These structures were then converted to PDB format using Open Babel version 2.5.7. Subsequently, the ligands were prepared for docking by generating PDBQT files, defining spatial parameters of the grid, and setting docking parameters. For the receptor, Kollman's partial charges and polar hydrogen atoms was incorporated into the 3ERT receptor structure to prepare it for docking. The docking grid was defined with dimensions of 80 × 90 × 80 points along the x, y, and z axes, respectively. The prepared receptor structure was subsequently stored in PDBQT format. The binding affinities of the ligands were expressed as negative Gibbs free energy (ΔG) values in kcal/mol are illustrated in Table 11. These values reflecting both the strength and thermodynamic favourability of the ligand–receptor interactions. Post-docking analysis was conducted using Discovery Studio, which enabled visualization of binding sites, hydrogen bonds, hydrophobic interactions, and bond distances within the docked complexes.

### *In vitro* antimalarial efficacy assay

**Parasite Culture Procedure**: *Plasmodium falciparum* strains Thailand (Thai) and K1 was employed for *in vitro* cell culture experiments[36]. The parasites were maintained in RPMI 1640 medium enriched using 11 mM glucose, 27.5 mM sodium bicarbonate, 100 U/mL penicillin, 100 µg/mL streptomycin, and 8% heat-inactivated human serum albumin. Cultures were incubated at 37 °C using human $A^+$ erythrocytes at a 2% haematocrit under a gas mixture containing 3% $CO_2$, 6% $O_2$, and 91% $N_2$. *In vitro* assays were conducted with parasite cultures exhibiting 3–6% parasitaemia, which was quantified using Giemsa-stained blood smears. Serial dilutions of the prepared imine derivatives were prepared in dimethyl sulfoxide (DMSO) and evaluated for their antagonistic activity on the intra-erythrocytic development of *Plasmodium falciparum*. Parasite cultures were incubated at 37 °C for 24 hours in a candle jar environment. Subsequently, 0.5 µCi of [$^3$H]-hypoxanthine were added to each well. Following a further 24-hour incubation period, the plates was subjected to freeze–thaw cycles and the contents were isolated onto filter membranes. The desiccated filters were soaked in a scintillation cocktail, and radioactivity was measured using a 1450 Micro-Beta liquid scintillation counter. Growth retardation was quantified based on the level of parasite-associated radioactivity, with 100% [$^3$H]-hypoxanthine incorporation representing the untreated control group in the lack of imine compounds.

$$\text{Inhibition concentration (\%)} = \frac{\text{Number of schizonts in test sample}}{\text{Number of schizonts in control}} \times 100$$

The half-maximal inhibitory concentration ($IC_{50}$) values for each compound were determined from the inhibition assays. Mean $IC_{50}$ values were calculated based on three independent experimental replicates. Nonlinear regression method was calculated through GraphPad Prism software by plotting log-transformed compound concentrations against the corresponding percentage of inhibition. The antimalarial potential of the imine derivatives was inferred from the calculated $IC_{50}$ values.

**Measurement of Antimicrobial activity**

Antibacterial screening was conducted through the Bauer–Kirby disc diffusion method[37] at a concentration of 30 μg/mL, with Ceftazidime serving as the reference standard. The prepared compounds were evaluated due to their *in vitro* antibacterial efficacy opposed to four Gram-positive and four Gram-negative bacterial strains. The Gram-positive strains included *Bacillus subtilis*, *Enterococcus faecalis*, *Streptococcus pneumoniae*, and *Staphylococcus aureus*. The inhibitory potential of the Schiff bases was assessed based on the zone of inhibition[38-40] observed on agar plates. Anti-fungal potencies of the synthesized *E*-imines were evaluated with two gram-positive fungal strains are *Candida albicans, Penicillium chrysogenum* and the two gram-negative fungal strains are *Aspergillus niger*, *Aspergillus fumigatus.* and *Clotrimazole* was taken as a standard drug for this analysis.

**Conclusions**

Eco-friendly ultrasound-promoted synthetic methodology adopted for more than 80% yield of sixteen aryl *E*-amines were synthesised. The synthesized imines were examined using elemental (micro) analysis, analytical techniques, and various spectroscopic methods. The effect of solvents on the *E*-imines was studied and it reveals that the ethanol medium of the reaction gave more yields. The molecular structure of (*E*)-*N*-(2-bromobenzylidene)-2-(trifluoromethyl) benzenamine (**13**) was unambiguously confirmed through single-crystal X-ray diffraction spectrum. Density Functional Theory (DFT) computations were utilized to explore the optimized geometries, molecular electrostatic potential maps, and frontier molecular orbitals (FMOs) of the compounds. The calculated energy gap between HOMO and LUMO is 1.45 eV, suggesting strong inhibitory potential. Mulliken charge distribution analysis shown the compound **13** have a most negative charge, which act as donors in compound (Br1, F3, C6, C8, C16, C18, C22, C28) have positive charge. Molecular docking studies shown the top protein-ligand binding energy of compounds **1, 3, 6** and **16**. In addition, ADME predictions of compound **10** and **12** provides good pharmacokinetic and pharmacodynamic profiles. Anti-malarial activity measurement study shows the *E*-imines **6** and **16** shows more antimalarial activity. Here the +I effect of bromine, chlorine, mesomeric effect of methyl, -I effect of methoxy, anthracene and 2-thienyl groups enhances the antimalarial activity. Compounds **1, 2, 5, 8** and **13** shows moderate antimalarial activity. All imines show good and excellent antibacterial activities against their microbes. All *E*-imines exists excellent and good antibacterial potencies against *C. albicans* and *P. chrysogenum* antifungal strains. *E*-imines **1, 2, 8** and **13-16** were shown good anti-fungal activity against *A. niger strain* and *A. fumigatus strains.* Here the –I effect of methoxy, +I effect of bromine, chloride, anthracene ring, electronegative character of fluorine, positive character of nitro group and mesomeric effect of methyl groups enhanced the antifungal activity.

**Acknowledgments**

Authors thank (i). DST-NMR Facility, Department of Chemistry Annamalai University, Annamalainagar 608 002 for recording NMR spectra of all imines and (ii) RUSA-2, Field 1, Anti-Malarial Drug Synthesis, No. F3/RUSA/673/2022, dated 4-6-2022, Annamalai University, Annamalainagar-608002, for financial support.

**Supplementary Information**

The XRD data of E-imine (13) is available. Computational and docking analysis outcomes are also available in the supplementary files in the website http://nopr.niscpr.res.in/handle/123456789/58776.

**References**

1 Karthikeyan M S, Prasad D J, Poojary B, Bhat K S, Holla B S & Kumari N S, *Bioorg Med Chem,* 14 (2006) 7482.
2 Dinesh Kumar N, Suppuraj P, Mayavel P, Muthuvel I & Thirunarayanan G, *Mater Today Proceed*, 29 (2020) 1059.
3 Suresh R, Kamalakkannan D, Ranganathan K, Arulkumaran R, Sundararajan R, Sakthinathan S P, Vijayakumar S, Sathiyamoorthi K, Mala V, Vanangamudi G, Thirumurthy K, Mayavel P & Thirunarayanan G, *Spectrochim Acta Part A: Molecular and Biomol Spectros*, 101(2013) 239.
4 Singh K, Barwa M S & Tyagi P, *Eur J Med Chem*, 42 (2007) 394.
5 Vicini P, Geronikaki A, Incerti M, Busonera B, Poni G, Cabras C A & Colla P L, *Bioorg Med Chem*, 11 (2003) 478.
6 Sondhi S M, Singh N, Kumar, Lozach O & Meijer, *Bioorg Med Chem*, 14 (2006) 3758.
7 Cheng L, Tan, J, Luo H, Jin X, Dai F, Yang J, Qian Y, Li X & Zhou B, *Bioorg Med Chem Lett*, 20 (2010) 2417.
8 Narayana B, Ashalatha B V, Raj K K V, Kumari N S, *Ind J Chem*, 45 (2006) 2696.
9 Sinha N, Jain S, Tilekar A, Upadhayaya R S, Kishore N, Jana G H & Arora S K, *Bioorg Med Chem Lett*, 15 (2005) 1573.
10 Patole J, Shingnapurkar D, Padhyea S & Ratledge C, *Bioorg Med Chem Lett*, 16 (2006) 1314.
11 Kucukguzel I, Kucukguzel S G, Rollas S, Sanis G O, Ozdemir O I, Altug T & Stables J, *IL Farmaco*, 59 (2004) 893.
12 Wu J, Liu X, Cheng X, Cao Y, Wang D, Li Z, Xu W, Pannecouque C, Witvrouw M & Clercq E D, *Molecules*, 12 (2007) 2003.

13 Menendez J C, Daiaz M P, Bellever C & Sollhuber M M, *Eur J Med Chem*, 27 (1992) 61.

14 Tarafder M T, Kasbollah A, Saravan N, Crouse K A, Ali A M & Tin O K, *Biochem Mol Biol Biophy*, 6 (2002) 85.

15 Yadav R, Srivastava S D & Srivastava S K, *J Environ Sci Health*, 44 (2000) 428.

16 Kundu A, Shakil N A, Saxena D B, Kumar J P & Walia S, *J Environ Sci Health*, 44 (2000) 428.

17 Song H, Liu Y, Xiong L, Li Y, Yang N & Wang Q, *J Agric Food Chem*, 61 (2013) 8730.

18 Mayavel P, Divya J, Gayathri P, Balasundari S, Usha V, Muthuvel I, Krishnakumar B, Shivakumara K N & Gurusamy R, *Res Chem Intermed*, 50 (2024) 4503.

19 Digdem T, Muhammad A R**,** Necmi D, Aysen A A, Umme F & Shafiq U R, ACS Omega, 7 (2022) 10568.

20 Hasaninejad A, Zare A, Sharghi H & M. Shekouhy, *Arkivoc,* 11 (2008) 64.

21 Manikandan S & Thirunarayanan G, *Int J Appl Engg Res*, 13(2018)1077.

22 Dineshkumar N , Swaminathan M, Selvakumar K, Durai M, Muthuvel I, Ebaid H, Krishnakumar B, Young-Ho A & Thirunarayanan G, *J Mol Struct*, 1325(2025) 140918.

23 Muthuvel I, Dineshkumar S, Thirumurthy K, Krishnakumar B & Thirunarayanan G, *Indian J Chem*, 55B (2016) 252.

24 Ghouse S, Sreenivasulu C, Kishore D & Satyanarayana G, *Tetrahedron*,105, (2022) 11077.

25 Thirunarayan G, Mayavel P, Thirumurthy K, Vananagamudi G, Lakshmanan K & Sekar K. G, Int J Chem, 1(2012) 166.

26 Mala V, Muthuvel I, Thirunarayanan G & Usha V, *Mater Today Proceed*, 43 (2021) 2117.

27 Balaji S, Manikandan V, Rajarajan M, Usha V, Rajalakshmi S, Venkatachalam P, Muthuvel I & Thirunarayanan G, *Mater Today Proceed*, 42 (2020) 931.

28 Mayavel P, Thirumurthy K. Dineshkumar S & Thirunarayanan G, *Ind J Chem*, 54B (2015) 779.

29 Suresh R, Sakthinathan S P, Kamalakkannan D, Muthuvel I & Thirunarayanan G, *Ovidius Univ Annal Chem*, 31 (2020) 55.

30 Dineshkumar N, Muthuvel I & Thirunarayanan G, *Indian J Chem*, 62 (2023) 906.

31 Dineshkumar N, Thirunarayanan G, Elancheran R, Suppuraj P, Guganathan L, Sivasakthikumaran R, Ramkumar S & Swaminathan M, *J Mol Struct* 1322 (2025) 140603.

32 Nalini S*,* Gayathri P, Divya J, Muthuvel I, Thirumurthy K, Mayavel P & Dinesh kumar N. *Russ J Org Chem*, 60 (2024) 2242.

33 Koteswara Rao Anam & Thirunarayanan G, *Indian J Chem,* 62 (2023) 91.

34 Dinesh kumar N, Mayavel P, Muthuvel I & Thirunarayanan G, *Chem Data Coll,* 30 (2020) 100547.

35 Serdaroglu G, Uludag N & Ustun E, *Chem Select*, 9 (2024) e202400019.

36 Gayathri P, Muthuvel I, Mayavel P, Ranganathan K, Usha V, Mala V & Thirunarayanan G, *Ovidius Univ Annal Chem*, 36 (2025) 66.

37 Bauer A W, Kirby W M M, Sherris J C & Truck M, *Am J Clin Pathol*, 45(4) (1966) 493.

38 Dinesh Kumar N, Rajamohan K S, Selvakumar K, Rajamanickam D, Thirunarayanan G & Swaminathan M, *J Mol Struct*, 1339 (2025) 142824.

39 Gayathri P, Divya J, Muthuvel I, Usha V, Retna M & Thirunarayanan G, *Indian J Chem* 64 (2025) 670.

40 Venkatraman R, Divya J, Gayathri P, Muthuvel I & Thirunarayanan G, *Indian J Chem*, 64 (2025) 465